

Activated dissociation of H_2 on the Cu(001) surface: The role of quantum tunneling

Xiaofan Yu(于小凡), Yangwu Tong(童洋武), and Yong Yang(杨勇)
Citation: Chin. Phys. B, 2023, 32 (**10**): 108103. DOI: 10.1088/1674-1056/acd2b3
Journal homepage: http://cpb.iphy.ac.cn; http://iopscience.iop.org/cpb

What follows is a list of articles you may be interested in

Tuning the particle size, physical properties, and photocatalytic activity of Ag_3PO_4 materials by changing the Ag^+/PO_4^{3-} ratio

Hung N M, Oanh L T M, Chung D P, Thang D V, Mai V T, Hang L T, and Minh N V
Chin. Phys. B, 2023, 32 (**3**): 038102. DOI: 10.1088/1674-1056/ac84ce

Properties of B_4C-TiB_2 ceramics prepared by spark plasma sintering

Jingzhe Fan(范静哲), Weixia Shen(沈维霞), Zhuangfei Zhang(张壮飞, Chao Fang(房超), Yuewen Zhang(张跃文), Liangchao Chen(陈良超), Qianqian Wang(王倩倩), Biao Wan(万彪), and Xiaopeng Jia(贾晓鹏)
Chin. Phys. B, 2021, 30 (**3**): 038105. DOI: 10.1088/1674-1056/abd7d8

Low-temperature plasma enhanced atomic layer deposition of large area HfS_2 nanocrystal thin films

Ailing Chang(常爱玲), Yichen Mao(毛亦琛), Zhiwei Huang(黄志伟), Haiyang Hong(洪海洋), Jianfang Xu(徐剑芳), Wei Huang(黄巍), Songyan Chen(陈松岩), Cheng Li(李成)
Chin. Phys. B, 2020, 29 (**3**): 038102. DOI: 10.1088/1674-1056/ab6c4a

Density functional calculations of efficient H_2 separation from impurity gases (H_2, N_2, H_2O, CO, Cl_2, and CH_4) via bilayer g-C_3N_4 membrane

Yuan Guo(郭源), Chunmei Tang(唐春梅), Xinbo Wang(王鑫波), Cheng Wang(王成), Ling Fu(付玲)
Chin. Phys. B, 2019, 28 (**4**): 048102. DOI: 10.1088/1674-1056/28/4/048102

Controllable preparation of tungsten/tungsten carbide nanowires or nanodots in nanostructured carbon with hollow macroporous core/mesoporous shell

Xiao-Na Ren(任晓娜), Min Xia(夏敏), Qing-Zhi Yan(燕青芝), Chang-Chun Ge(葛昌纯)
Chin. Phys. B, 2017, 26 (**3**): 038103. DOI: 10.1088/1674-1056/26/3/038103

RAPID COMMUNICATION

Activated dissociation of H_2 on the Cu(001) surface: The role of quantum tunneling

Xiaofan Yu(于小凡)[1,2,†], Yangwu Tong(童洋武)[1,2,†], and Yong Yang(杨勇)[1,2,‡]

[1] *Key Laboratory of Photovoltaic and Energy Conservation Materials, Institute of Solid State Physics, HFIPS, Chinese Academy of Sciences, Hefei* 230031, *China*

[2] *Science Island Branch of Graduate School, University of Science and Technology of China, Hefei* 230026, *China*

(Received 28 February 2023; revised manuscript received 30 April 2023; accepted manuscript online 5 May 2023)

The activation and dissociation of hydrogen molecules (H_2) on the Cu(001) surface are studied theoretically. Using first-principles calculations, the activation barrier for the dissociation of H_2 on Cu(001) is determined to be ~ 0.59 eV in height. It is found that the electron transfer from the copper substrate to H_2 plays a key role in the activation and breaking of the H–H bond, and the formation of the Cu–H bonds. Two stationary states are identified at around the critical height of bond breaking, corresponding to the molecular and the dissociative states, respectively. Using the transfer matrix method, we also investigate the role of quantum tunneling in the dissociation process along the minimum energy pathway (MEP), which is found to be significant at or below room temperature. At a given temperature, the tunneling contributions due to the translational and the vibrational motions of H_2 are quantified for the dissociation process. Within a wide range of temperature, the effects of quantum tunneling on the effective barriers of dissociation and the rate constants are observed. The deduced energetic parameters associated with the thermal equilibrium and non-equilibrium (molecular beam) conditions are comparable to experimental data. In the low-temperature region, the crossover from classical to quantum regime is identified.

Keywords: H_2, Cu(001), dissociation, quantum tunneling, density functional theory (DFT), transfer matrix method

PACS: 82.37.Np, 82.65.+r, 68.43.–h, 66.35.+a **DOI:** 10.1088/1674-1056/acd2b3

1. Introduction

As a clean energy source, hydrogen mainly exists in the form of molecules in nature. Materials involving metal elements are commonly utilized as catalysts for hydrogen production and storage to harvest hydrogen-based energy.[1–3] The elementary dynamics (e.g., adsorption and diffusion) of hydrogen on transition metal surfaces are closely related to some important physical and chemical processes such as crystal growth, hydrogen embrittlement, and surface corrosion, as well as technological applications like radiation protection in fusion reactor, electrode reactions in fuel cells, and surface catalysis.[4–19] When H_2 molecules approach a metal surface, depending on the energetics, they may remain in the molecular form, or they can dissociate with the H atoms attached separately on the metal surface. The key factor determining the energetics is the energy path, in particular the energy barrier associated with the dissociation process, i.e., the dissociation barrier. It is found that the dissociation barriers of hydrogen molecules on metal surfaces depend on the types of metals. For instance, the H_2 molecules adsorbed on the surfaces of Pt and Rh can spontaneously decompose into H atoms.[20–22] By contrast, the H_2 molecules adsorbed on the surface of Cu and Ag[23] cannot decompose into H atoms spontaneously. Additional energy consumption is required for the dissociation process, which is usually referred to as an activated process, with an energy barrier $E_b > 0$, as compared with $E_b = 0$ for the spontaneous process. The dissociation barriers of hydrogen are also quite different for different crystallographic planes. The existence of an activation barrier is commonly believed to be due to the full occupation of d orbitals, which induces Pauli repulsion when molecules encounter surfaces.[24,25] Consequently, the dissociation processes of H_2 on the surfaces of the metals that have fully-occupied d orbitals tend to be activated processes ($E_b > 0$), while the dissociation on the metals with partially-occupied *d* orbitals is more likely to be a spontaneous process ($E_b = 0$). There have been many experiments reported[6,8,10,14,15] for the adsorption, dissociation and diffusion processes of hydrogen on different metal surfaces. For example, the nozzle beam experiment, with sticking coefficient measurements for monoenergetic molecular beams as a function of energy and the angle of incidence, was carried out to study the adsorption and desorption kinetics of H_2 on Cu surfaces.[6] Using thermal desorption with work function and low-energy electron diffraction (LEED) measurements, the adsorption state and adsorption energy for the H/Pd(100) system was determined.[8] Molecular beam techniques were

†These authors contributed equally to this work.

‡Corresponding author. E-mail: yyanglab@issp.ac.cn

© 2023 Chinese Physical Society and IOP Publishing Ltd

utilized to control the kinetic energy and the incident angle of H_2 molecules, and to explore in detail the nature of the dissociation barriers on copper surface.[10]

As a typical prototype system for the activated reactions of H_2 with metal surfaces, H_2/Cu has been the subject of immense theoretical investigations, primarily on the dissociation and sticking dynamics,[26–49] and the thermal desorption spectra,[50] which are directly related to the energy pathway governing the dissociation/desorption processes. Generally, the collision between a diatomic molecule with a surface involves at least six degrees of freedom, if the surface is as assumed to be rigid. For an accurate description of the process, a study of six-dimensional (6D) dynamics is usually required. Such a study is feasible for classical mechanics, but it is relatively challenging for quantum-level simulations. Based on the potential energy surface (PES) constructed within the Born–Oppenheimer approximation, multi-dimensional (3D to 6D) quantum dynamics calculations have been carried out to study the activated dissociation of H_2 on Cu surfaces,[28–41] with a focus on the role of the vibrational and rotational states of H_2, as well as the coupling between both degrees-of-freedom.[29–40] Using 6D quantum simulations, it is found that[33–35] the dissociation probability depends on the orientation of the axis-of-rotation of the incident H_2 molecule. The so-called "helicopter" orientation (where the angular momentum vectors are perpendicular to the surface, or the line joining the H–H bond is parallel to the surface) yields a reaction probability that is dramatically larger than for the "cartwheel" orientation, where the angular momentum vectors of H_2 are parallel to the surface. Recently, special attention has been paid to the development of chemically-accurate PES for the interactions between H_2 and the copper and other metal surfaces.[42–49] Notable progress in this field includes, for instance, the implementation of the semi-empirical specific reaction parameter (SRP) approach to the density functional theory (DFT),[42–47] and the recently-developed machine learning PES.[48,49]

As compared with other elements, hydrogen has a smaller mass, and therefore more significant nuclear quantum effects are expected in its dynamical process.[51–54] In recent years, the important role of atomic quantum tunneling in the reaction rates and the selectivity of chemical processes involving small molecules has been increasingly reported.[55,56] For instance, it is found that nuclear quantum effects account for the facile activation and dissociation of H_2 on Cu(111) surface which is alloyed with 1% monolayer of Pd.[57,58] Analysis based on model potentials has shown that quantum tunneling is essential to the sticking of H_2 on metal surfaces.[26] Despite the enormous number of experimental and theoretical investigations, there still lack of systematic and in-depth studies on the role of quantum tunneling in the activated dissociation of H_2 on metal surfaces. In this paper, we revisit this topic by studying the activation and dissociation of H_2 molecules on Cu(001). The effects of quantum tunneling are investigated based on first-principles calculations combined with the transfer matrix method, for which the minimum energy pathway (MEP) of dissociation is extracted from *ab initio* potential energy surface (PES). During the activation process of H_2 on Cu(001), it is shown that the charge transfer between the Cu surface and the H_2 molecules is the key for the breaking of H–H bond and the formation of Cu–H bonds. Bistability of the adsorption states is identified in the vicinity of the critical point of dissociation. The probability of dissociation and the corresponding rate constants due to the translational (H_2 tunneling as a whole unit) and the vibrational motions of H_2 molecules are quantitatively evaluated. The obtained activation barrier and the threshold kinetic energy for detectable dissociation events agree with experimental observations. The effective dissociation barrier is evaluated as a function of temperature, whose magnitude is found to be significantly reduced owing to the quantum tunneling of H atoms. For the dissociation of hydrogen isotopes H_2 and D_2, the crossover from the high-temperature classical dynamics to low-temperature quantum dynamics is recognized.

This paper is organized as follows. Following the introduction, Section 2 presents the technical details of the first-principles calculations and the transfer matrix (TM) method employed in this study. In Section 3, the results for the energy path of the activated dissociation of H_2 on Cu(001), the role of charge transfer, and the role of quantum tunneling in shaping the kinetic process are presented and compared with experiments. Section 4 summarizes the main findings of this paper.

2. Methods

2.1. First-principles calculations

The Vienna *ab initio* simulation package (VASP)[59,60] based on density functional theory (DFT) is employed for the first-principles calculations. The Perdew–Burke–Ernzerhof (PBE) functional within the generalized gradient approximation (GGA)[61,62] is used to describe the exchange correlation of electrons, in combination with the PAW potentials[63,64] to describe the electron–ion interactions. The energy cutoff for the plane-wave basis sets is 600 eV. The initial atomic configurations are constructed with the aid of VESTA,[65] which models the Cu(001) surface as a six-layer $p(3\times3)$ supercell repeating periodically along the xy plane with a vacuum layer of about 15 Å along the z direction. In all the calculations, the Cu atoms in the bottom three layers are fixed while the atoms in the upper layers are relaxed. We employ a dipole correction for the total energy to eliminate the artificial dipole–dipole interaction caused by the upper and lower asymmetric slab surfaces. A $4\times4\times1$ Monkhorst–Pack k-mesh[66] is generated to

sample the Brillouin zone (BZ) in performing structural relaxation and total energy calculations. These sets of parameters ensure the total energy calculations converge within an error bar of ~ 0.5 meV/atom. The vibrational properties of the relaxed structures are analyzed using the density functional perturbation theory (DFPT).[67]

2.2. Transfer matrix method

The probability of a quantum particle passing through a potential barrier of arbitrary shape can be obtained using the transfer matrix (TM) method. By numerically slicing an arbitrarily-shaped potential, it is transformed into a stack of multiple rectangular potential barriers (potential wells).[54] The transmission of a particle through each rectangular potential barrier (potential well) can be represented by a matrix of coefficients that describe the transmitted and the reflected amplitudes of the wave function. Multiplying the coefficient matrices in turn one obtains a transition matrix representing the transition relationship between the initial and the final states. For the transmission across a potential $V(x)$, the incoming ($A_{\rm L}$, $B_{\rm L}$) and outgoing amplitudes ($A_{\rm R}$, $B_{\rm R}$) of the wave functions can be related as follows:[54]

$$\begin{pmatrix} A_{\rm R} \\ B_{\rm R} \end{pmatrix} = M \begin{pmatrix} A_{\rm L} \\ B_{\rm L} \end{pmatrix}, \tag{1}$$

where $M \equiv \begin{pmatrix} m_{11} & m_{12} \\ m_{21} & m_{22} \end{pmatrix}$ is the transfer matrix. In a system that preserves the time-reversal symmetry, the determinant is $|M| = 1$, and the transmission coefficient is calculated by $T_{\rm r}(E) = 1/|m_{22}|^2$.

The advantage of the TM method is that the obtained transmission probabilities are numerically accurate as compared with that calculated by the Wentzel–Kramers–Brillouin (WKB) approximation.[68] For instance, when the incident energy of a classical particle is higher than the potential barrier, the probability of the particle passing through the barrier is 1. Such a deficiency of traditional WKB is partly amended by an improved version.[69] For a quantum particle, due to the existence of quantum interference, even if the energy of the particle is greater than the barrier height, there may be a certain probability of reflection, which makes the probability of passing through the potential barrier to be smaller than 1. The TM method deals with the transport of quantum particles through a given potential field in a unified manner, and it fully considers the quantum effects in the process of crossing a potential barrier.

3. Results and discussion

3.1. Mechanistic analysis of the interaction between H_2 and Cu(001)

We begin by investigating the atomistic process of the dissociation and adsorption of H_2 on the Cu(001) surface. Figure 1 shows some typical configurations representing the dissociation process of a H_2 molecule approaching the Cu(001) surface along the normal (z) direction. The orientation line of H–H bond is parallel to Cu(001), and the midpoint of H–H bond is right above one of the bridge sites of Cu(001), with the projection of H–H bond perpendicular to the surface of Cu–Cu bond. Such an initial configuration gives rise to the largest possibility of dissociation.[17,25,33–35] Our calculations found that, when the distance between the H_2 molecule and the Cu(001) surface decreases to a critical value ($z_{\rm c} = 0.947$ Å), the covalent bonds in the H_2 molecules tend to break, and the molecule decomposes into two adsorbed H atoms on the Cu(001) surface. The corresponding PES is obtained by the following procedure: At the height of the center-of-mass Z_{H_2}, the H_2 bond length $d_{\rm H-H}$ is gradually varied, and the configuration space is sampled point-by-point with the energy of each configuration at the coordinates (Z_{H_2}, $d_{\rm H-H}$) given by the DFT calculations. The PES is shown in Fig. 2(a), with its 2D projection onto the parameter plane Z_{H_2}–$d_{\rm H-H}$ shown as a contour plot in Fig. 2(b). The MEP is indicated by the scattered dots in Figs. 2(a) and 2(b), with four typical configurations labeled by A, B, C, and D. The top and side views

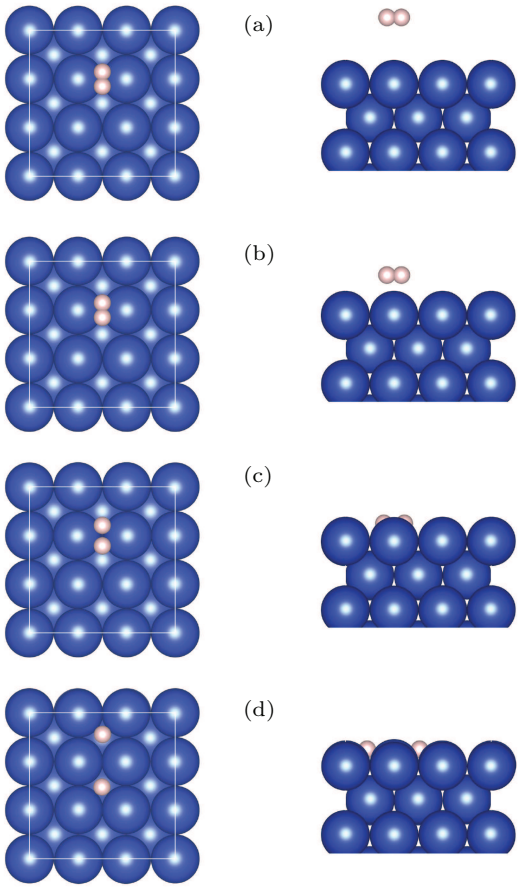


Fig. 1. Top (left) and side views (right) of the typical H_2/Cu(001) configurations, from the molecular state (a) to the dissociative state (d). The blue (large) balls represent Cu atoms, while the pink (small) ones are for H atoms. This convention applies to all the figures.

of the MEP are schematically shown in Fig. 1. The relative energy with respect to the initial molecular state (configuration A) is shown in Fig. 2(c), as a function of the distance ($|Z_0 - Z|$) traveled by the center-of-mass of H_2 approaching the Cu(001) surface. Compared to Figs. 2(a) and 2(b), the relative energies for the configurations near the critical point shown in Fig. 2(c) are refined by the calculations with relaxed H_2 bond length (d_{H-H}) at a given height Z_{H_2}. Therefore, the refined MEP represents a set of energy local minima along the reaction path. Figure 2(d) shows the variation of total energy E_0 (with respect to configuration A) as a function of the bond length d_{H-H} at a series of heights z ($= Z_{H_2}$), from the gaseous molecular state ($z \sim 2.813$ Å) to near the critical height of dissociation ($z_c \sim 0.947$ Å). The local minima of the curves correspond to the dynamically stable configurations locating on the MEP, yielding the stable bond lengths d_{H-H} at a given height. Compared with the other E_0–d_{H-H} curves of molecular state, the most remarkable feature of the curve ($z = 0.968$ Å) at the vicinity of the critical height ($z_c = 0.947$ Å) is the existence of two stationary points, as indicated by the two local minima at $d_{H-H} = 0.990$ Å and 2.772 Å, respectively. The two minima are separated by a small barrier of $\Delta E \sim 3$ meV. This small barrier implies that a weak perturbation will switch the molecular state (C) to the dissociative state (C_d), leading to an abrupt change in the bond length d_{H-H}. At temperatures $T \leq 300$ K, the H_2 molecule is frozen at its vibrational ground state, and the translational motion along the surface normal direction (z) therefore plays a major role. Near the critical height, a slight increase in the kinetic energy of the center-of-mass and consequently a small decrease in the H_2-Cu(001) distance will result in an abrupt breaking of the H–H bond.

Before the onset of the dissociation, the energy of the system continuously rises with the decreasing of H_2-Cu(001) distance. At the critical point of bond breaking, there is a sudden change, and the energy of stationary states drops abruptly, as indicated by the C–C_d line shown in Fig. 2(c). Accordingly, the energy drop (from configuration C to D) in this process corresponds to the desorption barrier of chemically-adsorbed H on Cu(001). The height of the barrier ($E_b \sim 0.586$ eV) is in good agreement with that from the previous works ($E_b \sim 0.58$ eV)[17,46,70] at the GGA level, but it is lower than the barrier height ($E_b \sim 0.74$ eV) calculated using the SRP-DFT method.[43,45,46] The desorption barrier and the desorption rate of H_2 on the Cu(001) surface[15] are commonly measured in experiments using temperature-programmed desorption (TPD); they can be numerically simulated based on the DFT calculations in combination with kinetics analysis.[50]

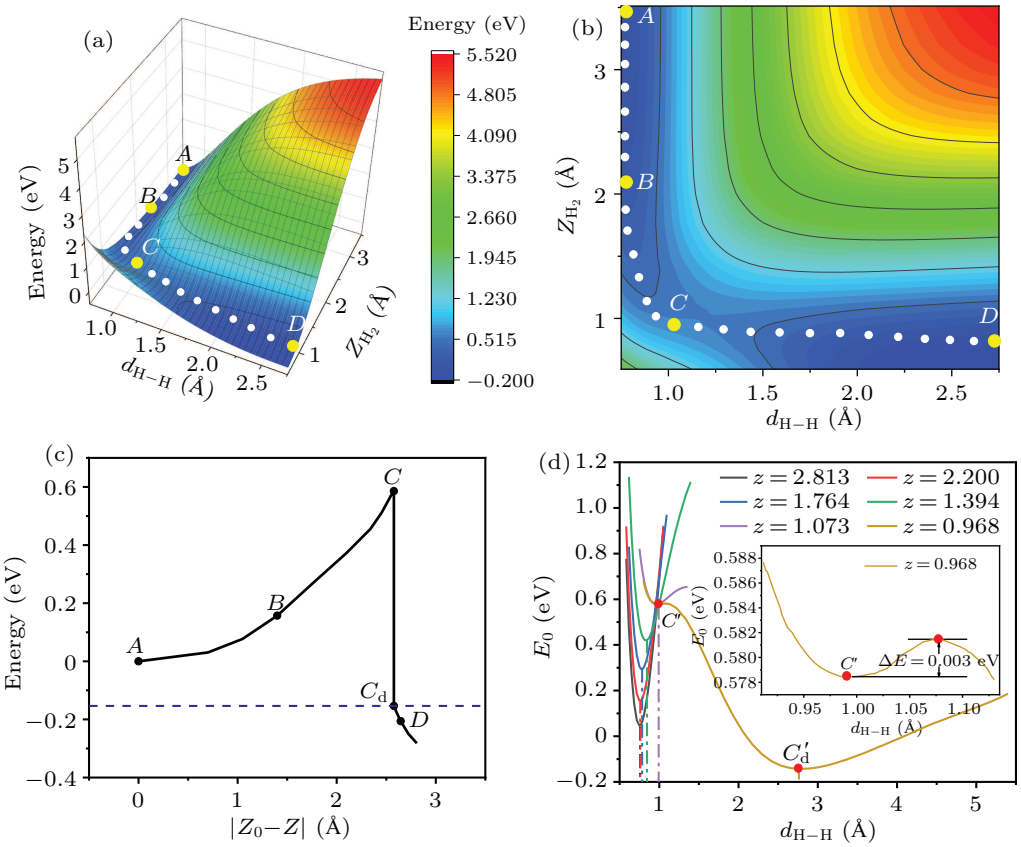


Fig. 2. Calculated PES (a), its 2D contours (b), and the refined MEP (c) for the activated dissociation of H_2 on the Cu(001) surface. (d) Variation of the relative energy (E_0) with the bond lengths (d_{H-H}) at a given height z. The energy of the initial configuration at gaseous phase (configuration A) is set as zero point. The points A–D in (c) correspond to the atomic configurations shown in Figs. 1(a)–1(d), respectively. Z_0 is the initial height of H_2 and $|Z_0 - Z|$ is the distance traveled. The points C and C_d represent the two stationary states at the critical height z_c.

To understand the bond breaking from the level of electron, we have calculated the charge density differences for a number of typical adsorption configurations, including the initial molecular state, the intermediate and transition states of dissociation, and the final fully-dissociated state on Cu(001). Practically, the charge density difference ($\Delta\rho$) of a given configuration is obtained by subtracting the charge density of the substrate and two individual H atoms from the total charge density of the adsorption system. The formula is as follows:

$$\begin{aligned}\Delta\rho \;=\; & \rho[\mathrm{H_2/Cu(001)}] - \rho[\mathrm{H_1}] \\ & - \rho[\mathrm{H_2}] - \rho[\mathrm{Cu(001)}],\end{aligned} \tag{2}$$

where $\rho[\mathrm{H_2/Cu(001)}]$ is the charge density of the system of H_2/Cu(001), $\rho[\mathrm{H_1}]$ and $\rho[\mathrm{H_2}]$ denote respectively the charge densities of the two H atoms, $\rho[\mathrm{Cu(001)}]$ is the charge density of the Cu(001) system.

The isosurfaces of charge density differences are shown in Fig. 3. When the H_2 molecule is far away from the Cu(001) surface, there is no charge transfer between H_2 and the substrate. Instead, one sees mainly the charge difference with positive values in-between the two H atoms (Fig. 3(a)), which is a clear evidence of the H–H covalent bond. As the distance between H_2 and Cu(001) decreases, the electrons from substrate Cu start to be transferred to the H atoms. The closer they are, the larger the amount of charge transfer is found. When the H_2–Cu(001) distance is $z = 0.749$ Å, the two H atoms are separated from each other and the H–H covalent bond is broken. The H atoms are located between four nearest neighboring Cu atoms and exchange charges with them. The H atoms gain electrons while the Cu atoms lose electrons. The electrons gather around the H atoms, indicating some characteristics of ionic bond between H and Cu atoms. Figures 4(a)–4(d) show the two-dimensional (2D) contours of charge distributions, which are sliced along the surface normal plane through the centers of the two H atoms. When the H_2–Cu(001) distance is $z = 0.592$ Å, the covalent bond is completely broken. It is worth noting that the H–H bond is very weak at $z_c = 0.947$ Å, but it is still not broken. This can be regarded as the critical state. The breaking of the H–H bond is observed instantaneously when the H_2–Cu(001) distance exceeds the critical value ($z_c = 0.947$ Å).

To get more insights into the dynamical process associated with charge transfer, we study the charge transfer between H_2 molecule and the substrate using the Bader analysis.[71] The results are shown in Fig. 4(e). When an H_2 molecule gradually approaches the Cu(001) surface, electrons from the underlying Cu substrate are gradually transferred to the two H atoms. The critical distance between the hydrogen molecule and the surface of Cu(001) is $Z_{\mathrm{H_2-Cu(001)}} \approx 0.947$ Å, corresponding to a decrease in the height $|Z_0 - Z| \approx 2.576$ Å. As seen from Fig. 2(c), the total energy of the system drops steeply at this distance. Meanwhile, a sharp increase in the charge transfer to H atoms is observed (Fig. 4(e)). The abrupt changes in both the total energy and the number of transferred electrons indicate that the dissociation of hydrogen molecules at the critical point may be an ultrafast process.

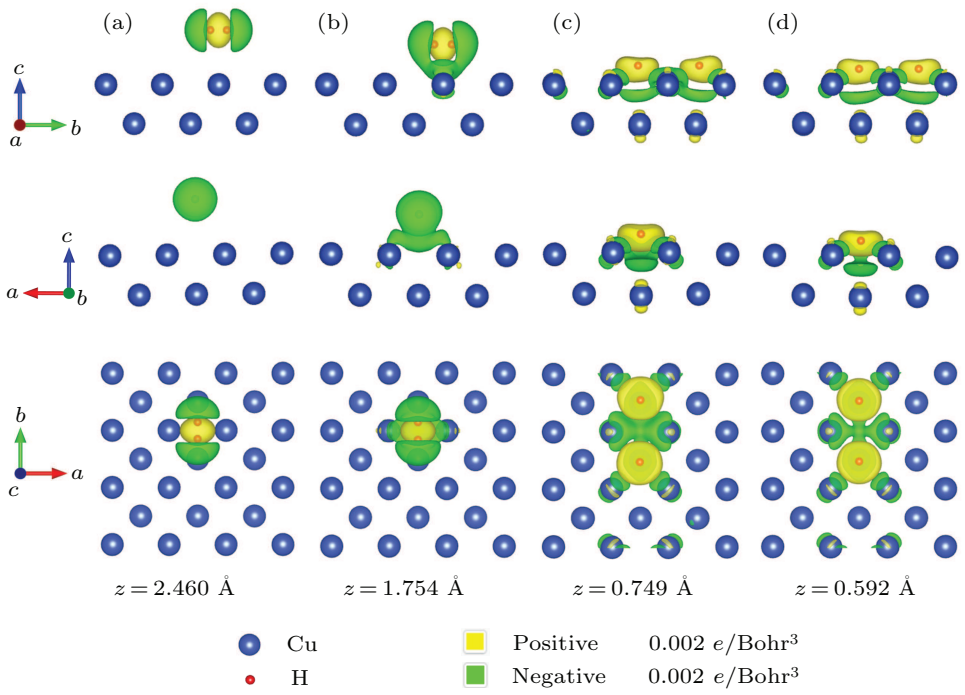


Fig. 3. Isosurfaces of the charge density differences for the H_2/Cu(001) at gradually decreasing H_2–Cu(001) distances. (a) The initial configuration of H_2, corresponding to the configuration in Fig. 1(a) and point *A* in Fig. 2(c). (b) The transition state of H_2 from the molecular to the dissociation states. (c) and (d) The dissociative states in the form of adsorbed H atoms on Cu(001), with (d) being the final stable dissociative state.

Figures 4(f)–4(i) show the variation of 2D charge distributions between one of the H atoms (the other one is geometrically equivalent) and the nearest neighboring Cu atoms. At the initial distance $z = 2.460$ Å, the H–Cu bond does not exist. As the distance between the H_2 molecule and the Cu(001) surface decreases, the H–Cu bond gradually forms and strengthens. Finally, the H atoms form H–Cu bonds with the nearest neighboring Cu atoms. The charge contours clearly demonstrate the formation of H–Cu bonds when a H_2 molecule approaches the Cu(001) surface.

From the analysis above, one may conclude that the adsorption and dissociation of H_2 molecules on Cu(001) is essentially a competition between H–H and H–Cu bonds. Regarding the forces governing this process, the nuclear (ion core)–electron interactions are attractive, while the nuclear (ion core)–nuclear (ion core) and electron–electron interactions are repulsive. The balance between the attractive and repulsive forces leads to the formation of the chemical bonds. The strength of the attraction is largely related to the extent of the overlap of electron wave functions. As a result, the strength of the attraction and the bonding between two atoms are largely determined by the overlap of wave functions of electrons that participate in the bond formation. For a given atom in a molecule, when the attraction from an atom of a foreign species is larger than that from the one it is bonded with, breaking of the old bond and the formation of a new bond are therefore expected.

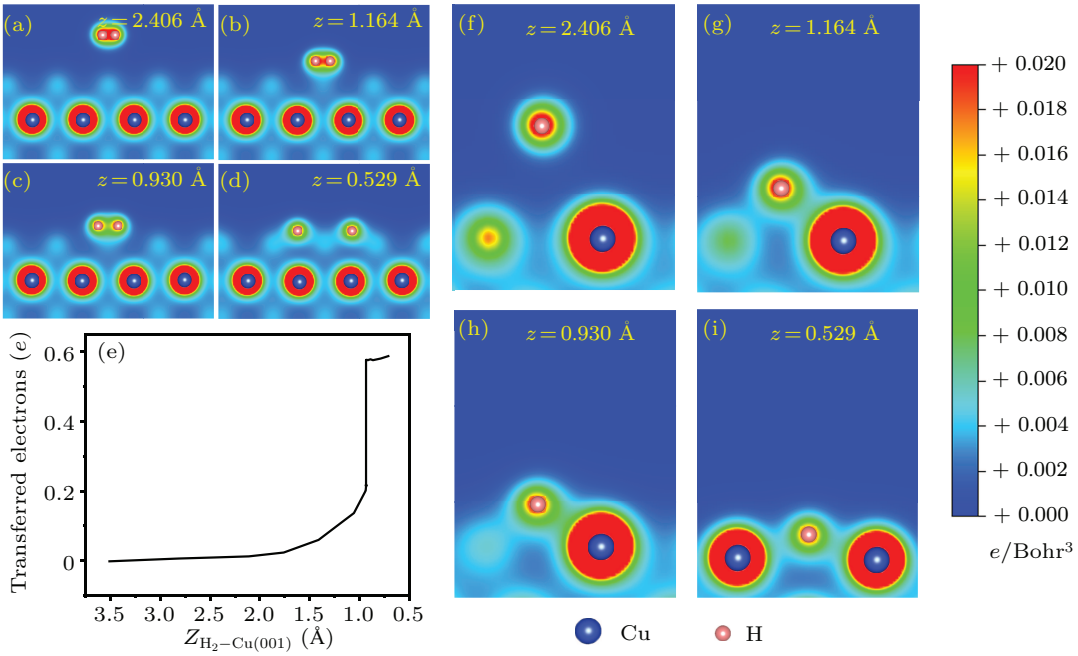


Fig. 4. The 2D contours of the charge densities associated with the breaking of H–H bond, from the molecular state (a), the transition states (b) and (c), to the dissociative state (d). (e) Charge transfer from Cu(001) to H_2, obtained from a Bader analysis, as a function of the distance from the center-of-mass of H_2 to Cu(001). (f)–(i) 2D contours of charge densities, illustrating the formation of H–Cu bonds for the same configurations as that for (a)–(d), but viewed from different perspective angles.

3.2. Role of quantum tunneling in the dissociation processes

For a hydrogen molecule incident on the Cu(001) surface, the line joining the H–H bond can be either parallel or perpendicular to Cu(001). Generally, the orientation of the H–H bonds with respect to the Cu(001) surface can be described by an angle α, which varies in the range of $0 \leq \alpha \leq 90°$. Previous studies based on semi-empirical and *ab initio* methods have shown that the barrier for H_2 dissociation on Cu(100) depends on the orientation angle.[17,33–35] Dissociation occurs more easily when the H–H axis is parallel to the surface. This is because the H_2 molecule of this orientation has the largest contact with the surface when it is close to the Cu(001) surface. Thus, it has the biggest chance of reaction and dissociation. Therefore, we only consider the case of $\alpha = 0$, for which the axis of the H–H bond is parallel to Cu(001), with the two H atoms and the center-of-mass sharing the same z coordinates. From the point of view of dynamical motions, the dissociation of H_2 molecules on Cu(001) is mainly due to the contribution of two processes. The first process is the dissociation due to the translational motion of H_2 in the vertical direction along the MEP, the most probable reaction path which is determined with the variation of H–H bond length (d_{H-H}) intrinsically included in our DFT calculations. As shown in Fig. 5(a), an H_2 molecule approaches the Cu(001) surface along the z direction by overcoming the potential barrier $U(z)$, i.e., the MEP, and finally it reaches the state of dissociation and chemisorption. The second process is the dissociation due to the stretching vibrations of H atoms in the horizontal direction (which

is parallel to the Cu(001) surface). These two processes consist with the concept of overcoming the early and the late barriers, respectively, in the dissociative attachment of diatomic molecules on surfaces.[72] As shown in Fig. 5(b), when the H atoms approach the Cu(001) surface along z direction, the lateral vibration of each H atom provides an additional probability of breaking the H–H bond by overcoming the lateral potential barrier $U(x, y)$. This can be determined by standard DFT calculations. For a given temperature T, the dissociation probabilities of the two processes can be calculated separately, and then the total dissociation probability is obtained by summing up the probabilities of the two processes. Unless otherwise stated, both H_2 molecules and single H atoms are treated as quantum particles in our study of the role of tunneling.

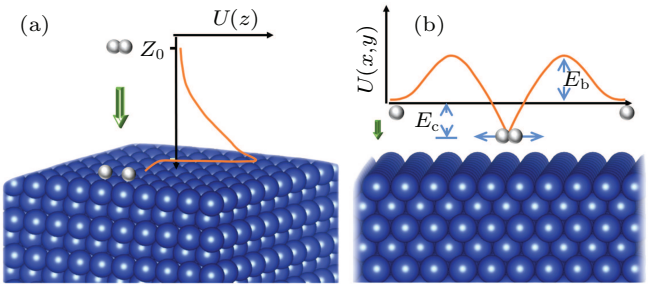


Fig. 5. Schematic diagrams for the dissociation of H_2 molecules incident along (a) the surface normal (z) directions and (b) the transverse direction. Here, Z_C and Z_0 correspond to the initial and the critical positions of H_2 (point C in Fig. 2), respectively. The potential energy difference between the instantaneous ground state of H_2 at height z and the zero point (completely dissociative state) of the potential energy is marked as E_c. The potential barrier height, with respect to the potential energy zero, is marked as E_b.

For the first process, the probability of dissociation is

$$P_{\perp}(T) = \int_0^{\infty} p(E,T)\,T_r(E)\,\mathrm{d}E \cong \int_0^{E_m} p(E,T)\,T_r(E)\,\mathrm{d}E, \tag{3}$$

where $p(E,T) = 2\pi(\frac{1}{\pi k_B T})^{3/2}\sqrt{E}\,\mathrm{e}^{-E/(k_B T)}$ is the kinetic energy distribution function;[73] it is suitable for the particles in thermal equilibrium systems where the parabolic momentum-energy relation exists and the scalar potentials dominate the interactions.[54] Here, T is the absolute temperature, E is the incident energy, and k_B is the Boltzmann constant. The quantity $T_r(E)$ is the transmission probability of the H_2 molecule (as a whole unit) across the potential barrier $U(z)$ (Fig. 5(a)), at a certain energy E; it is calculated by the transfer matrix (TM) method. In practice, an upper bound (E_m) is set for the evaluation of the integral, and it ensures the numerical results converge to desired precisions.

For the second process, the probability of dissociation is

$$P_{\parallel}(T) = \frac{1}{L}\int_{z_0}^{z_1}\mathrm{d}z\int_{U(z)}^{\infty} p(E,T)\,T_r(z)\,\mathrm{d}E \cong \frac{1}{L}\int_{z_0}^{z_1}\mathrm{d}z\int_{U(z)}^{E_m} p(E,T)\,T_r(z)\,\mathrm{d}E, \tag{4}$$

where z_0 is the initial height of H_2, and z_1 is the minimum height for H_2 to remain at molecular state (i.e., the critical height, z_c), as shown in Fig. 5(a). The length $L = (z_1 - z_0)$ is a normalization factor; it represents a decrease in the height with respect to Cu(001). The integration of the kinetic energy function is considered only for the case when $E \geq U(z)$. The quantity $T_r(z)$ is the probability that a H_2 molecule passes through the transversal potential $U(x, y)$ (Fig. 5(b)) at temperature T and height z; it can be obtained by the transfer matrix (TM) method combined with the calculations based on statistical mechanics. Quantum tunneling is possible only if the vibrational energy $E_n \geq E_c$, where E_c is the energy difference between the molecular and the dissociated states at a height z (Fig. 5(b)). The mathematical expression for the transmission probability is

$$T_r(z) = \sum_{n=n_c}^{\infty} p_n \times T_r(E_n - E_c, z), \tag{5}$$

where $p_n = \frac{\mathrm{e}^{-\beta E_n}}{Q}$, $\beta = \frac{1}{k_B T}$, $E_n = (n+\frac{1}{2})\hbar\omega$, $Q = \sum_{n=0}^{\infty}\mathrm{e}^{-\beta E_n} = \frac{\mathrm{e}^{\beta\hbar\omega/2}}{\mathrm{e}^{\beta\hbar\omega}-1}$, and E_n is the nth vibrational energy level of H_2 within the harmonic approximation (frequency ω). The value of $\hbar\omega$ can be obtained directly from DFPT calculations. Using the above expressions, the probability p_n can be expressed as

$$p_n = \mathrm{e}^{-n\beta\hbar\omega}(1 - \mathrm{e}^{-\beta\hbar\omega}). \tag{6}$$

The quantity $T_r(E_n - E_c, z)$ is the probability of a H_2 molecule passing through the transversal barrier $U(x, y)$ with an incident energy of $E_n - E_c$ and a height of z. Similarly, the transmission probability can be calculated using the TM method. The barrier height is E_b, as depicted in Fig. 5(b). For a numerical evaluation with energy sampling interval in the order of magnitude of 0.1 meV, a good convergence (with a relative deviation of less than 0.1%) of the integral is obtained when $E_m \approx 5E_b$.

At a given height z, the energy of the system is set to be the zero point of potential energy when the H–H bond is broken (Fig. 5(b)). The difference between the lowest potential energy point at this height and the potential energy zero is labeled as E_c. It should be emphasized that only the energy levels with $E_n \geq E_c$ can produce effective quantum tunneling, and the corresponding vibrational energy level is labeled as the n_cth excited state. The subscript of the summation is therefore $n \geq n_c$. In the case of $E_n < E_c$, evanescent waves of incident particles are expected, and the waves decay exponentially with the distance traveled. Finally, at temperature T, the total probability of H_2 dissociation on Cu(001) as a quantum particle is given by $P_Q(T) = P_{\perp}(T) + P_{\parallel}(T)$.

The role of quantum tunneling can be demonstrated by assuming the H_2 molecule to be a classical particle and then

comparing the probabilities of dissociation at given temperatures. The dissociation can be considered to be due to the contributions from two processes. The first process is to overcome the potential barrier $U(z)$ to reach the decomposed adsorption state when H_2 gradually approaches the Cu(001) surface along the z direction. The probability corresponding to this process can be calculated as follows:[53]

$$P_{C\perp} = \int_{E_{b\perp}}^{\infty} p(E_k)\,dE_k = \left(1 - \mathrm{Erf}\left[\sqrt{E_{b\perp}/(k_B T)}\right]\right) + \frac{2}{\sqrt{\pi}}\sqrt{E_{b\perp}/(k_B T)}\,e^{-(\frac{E_{b\perp}}{k_B T})}. \quad (7)$$

As mentioned above, $p(E_k) = 2\pi(\frac{1}{\pi k_B T})^{\frac{3}{2}}\sqrt{E_k}\,e^{-E_k/(k_B T)}$ is the kinetic energy distribution function at a given temperature T, E_k is the kinetic energy, and $E_{b\perp}$ corresponds to the height of $U(z)$, which is ~ 0.586 eV.

The second process is the dissociation due to the thermal motions of a single H atom overcoming the constraint of H–H bond. The probability of this process is given by $P_{C\parallel} = \exp(-\frac{E_{b\parallel}}{k_B T})$, where $E_{b\parallel} = E_{H-H}$ is the H–H bond energy, which was experimentally determined to be ~ 436 kJ/mol or 4.51 eV.[74] This value is well above $E_{b\perp}$ and thus one has $P_{C\perp} \gg P_{C\parallel}$. Therefore, the dissociation in the horizontal direction is negligible as compared with that in the vertical (surface normal) direction due to the translational motions of H_2. In summary, as a classical particle, the dissociation probability of H_2 is given by $P_c = P_{C\perp} + P_{C\parallel} \cong P_{C\perp}$. The calculated transmission probabilities are presented in Fig. 6, as a function of temperature. It is seen that both quantum and classical probabilities increase with elevating temperatures. Below $T = 1350$ K, the transmission probability considering quantum tunneling effects (P_Q) is always higher than that for the case of treating the H_2 molecule as a classical particle (P_C). This phenomenon is even more pronounced at room temperature and below, at which the quantum transmission probability P_Q is well above its classical counterpart P_C. In the lower panels of Fig. 6 the contributions of the two processes are compared. It is found that the first process plays a major role in the overall dissociation, especially at low temperatures. At $T \leq 18$ K, the probability of the first process is more than 100 orders of magnitude higher than that of the second one. In low energy region, the corner-cutting effects,[75–79] due to which the tunneling pathway deviates from the MEP, can be important for H_2 dissociation. Such effects have been partly included in the calculation of MEP, for which the constraint of symmetric configurations of H_2 is imposed (see texts above).

Using the calculated dissociation probability of the H_2 molecule on Cu(001), we can estimate the rate constants of dissociation. The reaction rate constant k can be obtained via the relation,[54] $k = \nu P$, where ν is the attempting frequency and P is the corresponding dissociation probability. For the first process, ν can be expressed as the reciprocal of the time $\tau(E)$ for traveling from the starting point z_0 to the end point z_1 (Fig. 5(a)). The dissociation rate constant for the first process is

$$\nu_\perp(E) = \frac{1}{\tau(E)} = \frac{1}{\int_{z_0}^{z_1}\sqrt{\frac{m}{2(U(z)-E)}}\,dz}, \quad (8)$$

where E is the kinetic energy of the incident particle, $U(z)$ is the dissociation potential along the vertical direction as shown in Fig. 5(a), and m is the mass of H_2 molecule. The traversal time $\tau(E)$ of tunneling across the barrier is obtained using Eq. (2) presented in Ref. [80]. The reaction rate constant of the first process is

$$k_\perp(T) = \int_0^{\infty} \nu_\perp(E)\,p(E,T)\,T_r(E)\,dE \cong \int_0^{E_m} \nu_\perp(E)\,p(E,T)\,T_r(E)\,dE. \quad (9)$$

Here, $E_m = 5E_b$ for the numerical evaluation of the integral, and $p(E,T) = 2\pi(\frac{1}{\pi k_B T})^{3/2}\sqrt{E}\,e^{-E/(k_B T)}$ for the kinetic energy distribution at temperature T.

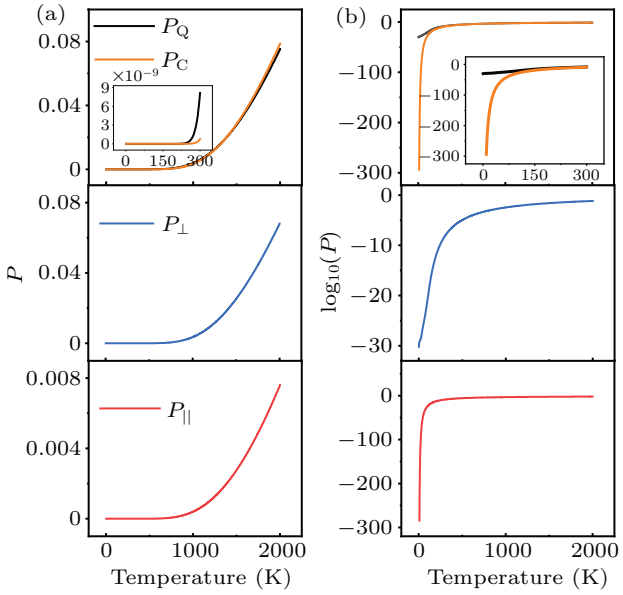


Fig. 6. The probability of H_2 dissociation due to the translational motions in surface normal direction (subscript $\perp$) and the vibrations in the transverse direction (subscript $\parallel$) on Cu(001), presented in both linear (a) and logarithmic scales (b). The classical (P_C) and the quantum probabilities (P_Q), as functions of temperature, are compared in the top panels.

For the second process, the frequency of the H–H stretching mode in the transverse direction, $\nu_\parallel(z)$, is used in the calculation of the rate constant. The frequency varies with the height z, in fact, it gets progressively smaller with decreasing height z. The rate constant for the second process is given by

$$k_\parallel(T) = \frac{1}{L}\int_{z_0}^{z_1} dz \int_{U(z)}^{\infty} \nu_\parallel(z)\,p(E,T)\,T_r(z)\,dE \cong \frac{1}{L}\int_{z_0}^{z_1} dz \int_{U(z)}^{E_m} \nu_\parallel(z)\,p(E,T)\,T_r(z)\,dE, \quad (10)$$

where the vibrational frequency $\nu_{\parallel}(z)$ can be obtained from the DFPT calculations. Ultimately, the total rate constant is

$$k_{\mathrm{Q}} = k_{\perp}(T) + k_{\parallel}(T). \tag{11}$$

The results for the rate constants are shown in Fig. 7, indicating that the dissociation in the vertical direction dominates the whole process. On the other hand, it is seen that (insets of Fig. 7) the dissociation due to the H–H vibrations (horizontal stretching) plays a nontrivial role at $T \geq 300$ K, for which both the translational and the vibrational motions of H_2 contribute significantly to the breaking of H–H bond.

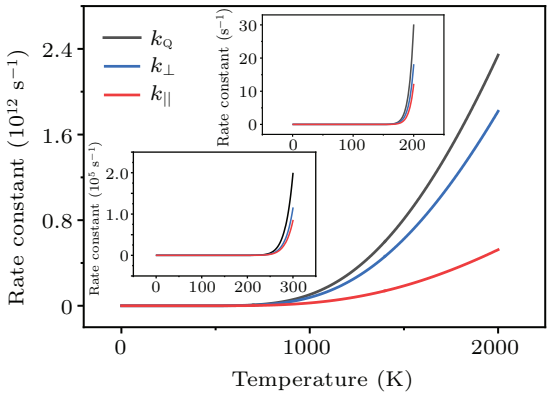


Fig. 7. Temperature dependence of the quantum rate constant k_{Q}, and their vertical and transverse components.

At the temperature $T_{\mathrm{d}} = 220$ K (insets of Fig. 7), the rate constant of dissociation is $k_{\mathrm{Q}} \sim 300/\mathrm{s}$, which corresponds to a dissociation number of $N_{H_2} \approx 1.08 \times 10^6$ within one hour. The smallest face-centered two-dimensional (2D) surface unit cell for Cu(001) is a square with the size $a \sim 3.61$ Å and the surface area $S_{\mathrm{Cu(001)}} = a^2 \cong 13.03$ Å^2. Periodically extending 1000 times along the two basis vectors yields a square substrate with a side length of $L \sim 0.361$ μm, which is comparable to the size of the samples employed in experiment. On average, each 2D surface unit cell can adsorb 1.08×2 H atoms. If we define a surface coverage of one monolayer (ML) for the adsorption of one H to one surface Cu atom, then at $T_{\mathrm{d}} = 220$ K, the surface coverage on Cu(001) within one hour is estimated to be ~ 1.13 ML. This coverage is experimentally measurable. Nontrivial dissociation of H_2 is expected to take place on Cu(001) at $T \geq T_{\mathrm{d}}$. The predicted temperature for the onset of the nontrivial dissociation of H_2 is $T_{\mathrm{d}} = 220$ K, which is comparable to previous experimental observations of the thermal desorption of dissociated H from Cu(001) ($T_{\mathrm{d}} \sim 218$ K).[15] A significant increase in the reaction rate constant is found when the temperature reaches 1000 K and above (Fig. 7). At such temperature the dissociation due to the stretching mode of H–H vibrations starts to play a nontrivial role. This is also in good agreement with the previous experimental measurements. When the kinetic energies of the hydrogen molecules ejected from the molecular beam nozzle reached about an equivalent temperature of ~ 1000 K and above, it was observed that hydrogen began to adsorb instantaneously on the copper surfaces with measurable sticking coefficients.[6]

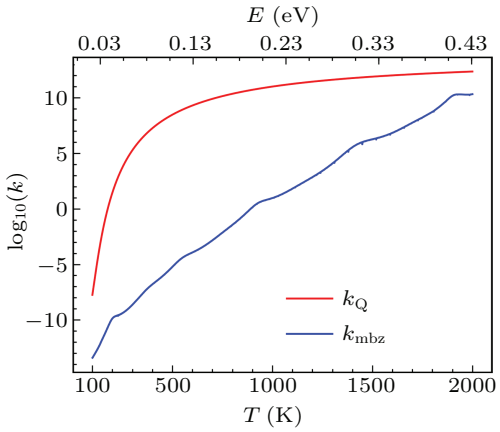


Fig. 8. Calculated rate constants k_{Q} and k_{mbz} (in logarithmic scales) for the dissociation of H_2 on Cu(001) under the thermal equilibrium condition and from molecular beam experiments, respectively.

The kinetic processes studied above are based on the precondition that the dosed H_2 molecules are in thermal equilibrium, with a well-defined kinetic energy distribution.[54] The situation changes significantly when the incident H_2 molecules are produced by a molecular beam nozzle,[6,10] where the kinetic energy of H_2 molecules has a very narrow distribution[10] and it can be as assumed to be single-valued. For the monoenergetic molecular beams of H_2 with kinetic energy E, the probability of tunneling is given by the transmission coefficient $T_{\mathrm{r}}(E)$, which is readily computed using the TM method. For a H_2 molecule which penetrates the barrier $U(z)$ and arrives at the Cu(001) surface, the rate constant of dissociation is $k_{\mathrm{mbz}}(E) = \nu_{\perp}(E) \times P_{\perp}(E) = \nu_{\perp}(E) \times T_{\mathrm{r}}(E)$. We have compared the rate constant of dissociation of H_2 under thermal equilibrium with that for the non-equilibrium molecular beam experiment. The characteristic temperature for the activation of the rotational degree-of-freedom of a H_2 molecule is $\theta_{\mathrm{r}} \sim 85$ K.[81] By contrast, the vibrational degree-of-freedom of H_2 is largely frozen at its ground state due to the very high characteristic temperature ($\theta_{\nu} \sim 6100$ K).[81] For temperatures above θ_{r}, both the translational and rotational degrees-of-freedom of H_2 are activated, and the equivalent temperature of the incident H_2 molecular beam with the kinetic energy E can therefore be estimated to be $T = 2E/(5k_{\mathrm{B}})$. The calculated rate constants are shown in Fig. 8, as a function of the temperature and the kinetic energy of each H_2 from molecular beams. It is clearly seen that at the same temperature the rate constant under thermal equilibrium (k_{Q}) is larger than that for molecular beams (k_{mbz}). Unlike the monoenergetic molecular beam with the translational kinetic energy E_{t}, the H_2 molecules at thermal equilibrium have a nontrivial probability of being at the energy states $E \geq E_{\mathrm{t}}$. This probability is

$P(E \geq E_t) = \int_{E_t}^{\infty} p(E)\,dE \cong \frac{2}{\sqrt{\pi}}\sqrt{E_t/(k_B T)}\,e^{-\left(\frac{E_t}{k_B T}\right)}$. Recalling that $E_t = \frac{3k_B T}{2}$, we have $P(E \geq E_t) \cong \frac{2}{\sqrt{\pi}}\sqrt{3/2}\,e^{-\left(\frac{3}{2}\right)} \cong 0.308$. This means that a considerable portion of H_2 molecules possess kinetic energies above the average E_t, and it also explains the difference between k_Q and k_{mbz}.

Using the experimental parameters presented in Ref. [10], i.e., the flux of the incident H_2 molecular beam through the nozzle (with the diameter $d = 3$ mm) is $\sim 10^{15}$ s^{-1}, and the number of incident H_2 molecules per second for unit area is estimated to be $F_{mbz} = \frac{N_{H_2}}{S_{mbz}} = \frac{N_{H_2}}{\pi(\frac{d}{2})^2} = \frac{10^{15}}{\pi \times 2.25 \times 10^{14}} \cong 1.41$ Å^{-2}. Within a time interval t, the number of H_2 molecules deposited on the surface unit cell of Cu(001) is therefore

$$n_{d,H_2}(E) = F_{mbz} \times S_{Cu(001)} \times k_{mbz}(E) \times t. \tag{12}$$

In the case $t = 1$ s, we have $n_{d,H_2}(E) \cong 18.4 \times k_{mbz}(E)$. For the kinetic energy $E = 0.176$ eV and $k_{mbz}(E) \cong 0.073$ s^{-1}, our calculations yield $n_{d,H_2}(0.176) \cong 1.3$, which implies that the surface coverage of dissociatively adsorbed H is ~ 1 ML. This is expected to give detectable signals for experimental measurements. The threshold value $E = 0.176$ eV for measurable dissociative adsorption of H_2 on Cu(001) is comparable to the experimental measurement $E = 0.2$ eV from molecular beam experiment.[6] This result shows the key role of quantum tunneling in the activated dissociation of H_2 on Cu(001).

3.3. Effective barrier and isotope effects

For the barrier-crossing process of a microscopic particle that satisfies the Van't Hoff–Arrhenius relation, the total transmission probability (P_{tot}) can be generally expressed as follows:[54]

$$P_{tot}(T) = e^{-E_b^*/(k_B T)}, \tag{13}$$

where E_b^* is the effective barrier, and $k_B T$ have the usual meanings as before. Therefore, the value of the effective barrier E_b^* can be obtained as follows:

$$E_b^* = -(k_B T)\ln[P_{tot}(T)] = k_B T \ln\left[\frac{1}{P_{tot}(T)}\right]. \tag{14}$$

Clearly, the effective barrier E_b^* is a function of temperature. Using the probability $P_{tot}(T)$ obtained by the TM method, the values of E_b^* at different temperatures are calculated, and the results are shown in Fig. 9. The data for the dissociation of H_2 and D_2 are presented, to show the isotope effects. It is seen that the effective barrier E_b^* , which includes the effects of quantum tunneling, is appreciably lower than the classical barrier height (dissociation along the surface normal, $U(z)$), which is deduced by treating the incident H_2 molecules as classical particles. For $T \geq 200$ K, the effective dissociation barriers of both H_2 and D_2 increase smoothly with T and reach their maxima at ~ 500 K, then they decrease slowly with further increasing temperatures. The nearly steady gap ($\Delta E = E_{bH2}^* - E_{bD2}^* \sim 0.02$ eV) between the effective barriers of H_2 and D_2 is a consequence of quantum tunneling, whose probability decreases with increasing particle mass. Our calculations found that, for $T \geq 1000$ K the gap (ΔE) decreases gradually and vanishes at ~ 3500 K, beyond which the system approaches the classical limit. The existence of a maximum for E_b^* can be qualitatively understood based on Eq. (14), where the competition between the terms $k_B T$ and $\ln\left[\frac{1}{P_{tot}(T)}\right]$ arrives at a compromise.[54] The weak temperature dependence of E_b^* at $T \geq 300$ K indicates that it is usually sufficient to use one barrier parameter to describe the temperature-dependent kinetic process of atoms.

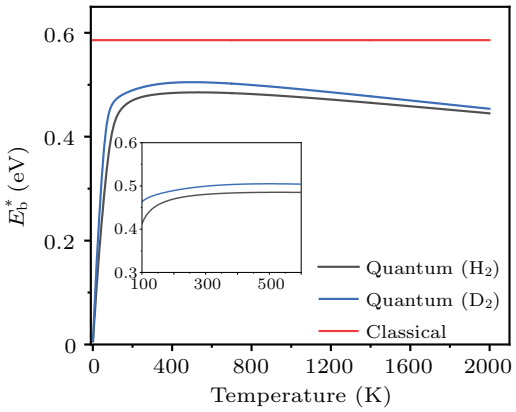


Fig. 9. The energy barriers for the dissociation of H_2 and D_2 on Cu(001). The original barrier height calculated using adiabatic approximation is referred to as "classical". The effective barriers (E_b^*) due to quantum effects are presented as a function of temperature.

The effective barriers for both H_2 and D_2 increase with temperature slightly, for $T \sim 200$ K to 260 K. In this temperature range, the barrier for H_2 varies from $E_b^* \sim 0.47$ at 200 K to 0.48 eV at 260 K. Similarly, the corresponding values for D_2 increase from 0.49 eV to 0.50 eV. This is comparable to the data from the thermal desorption (the reverse process of dissociation) measurements in the same temperature range, in which the activation barriers of dissociation are determined to be 48 ± 6 kJ/mol (or $\sim 0.50 \pm 0.06$ eV) for H_2 and 56 ± 8 kJ/mol (or 0.58 ± 0.08 eV) for D_2. The situation is much different for $T \leq 200$ K, where the effective barrier drops almost linearly with decreasing temperature. The effective barrier for H_2 decreases quickly from $E_b^* \sim 0.47$ eV at 200 K to 0.06 eV at 10 K, while the barrier for D_2 varies from 0.49 eV to 0.08 eV in the same temperature range. When the temperature T approaches 0, E_b^* tends to be zero, indicating that quantum tunneling effects may have a significant impact on the atomic-scale dynamics even at extremely low temperatures.

The significant role of quantum tunneling can be further demonstrated by investigating the isotope effects on the transmission probability and rate constant of H_2 and D_2 dissociation on Cu(001). In the calculations based on the TM method,

both H_2 and D_2 are treated as quantum particles, for temperature $T \leq 300$ K. The results are shown in Fig. 10. In the low temperature region, particularly for $T \leq 100$ K, significant differences between the transmission probabilities and rate constants are found. Using the relation $k = \nu P$, the natural logarithm of the reaction constant, $\ln(K_Q)$, may be expressed as follows:

$$\begin{aligned} \ln(K_Q) &= \ln(\nu P_Q) = \ln\left(\nu \mathrm{e}^{-\frac{E_b^*}{k_B T}}\right) \\ &= \ln\nu - \frac{E_b^*}{k_B T}, \end{aligned} \tag{15}$$

where the negative slope of the $\ln(K_Q) \sim \frac{1}{k_B T}$ line is simply due to the effective barrier E_b^* at a given temperature T. As seen from Fig. 10(d), at the turning point $T \sim 100$ K the rate constants for H_2 and D_2 depart from each other significantly, as an indication of the crossover from classical to quantum regimes. Moreover, the trends of the two curves can be roughly described by a combination of two lines that have the slopes being equivalent to the two effective barriers, as shown by the dash lines in Fig. 10(d). Similar characteristics of T-dependent rate constant are found in the case of H diffusion on the Cu(001) and Pt(111) surfaces;[82–84] these characteristics may be also expected for the diffusion processes on the surface of other metals. In the phenomenological description of the effects of quantum tunneling,[69,85] two sets of parameters for the activation barriers (for both classical and quantum motions) together with two prefactors are introduced to roughly account for the dynamics at high and low temperature regions. By contrast, our method produces the major features of the variations of rate constant with temperature in a logically natural and unified manner, and it provides a promising way for including quantum tunneling effects in the chemical dynamics of many-body systems.

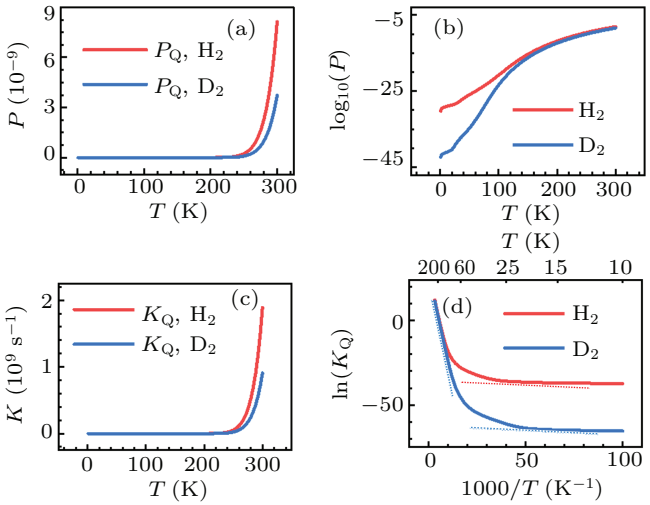


Fig. 10. Calculated quantum probabilities (upper panels) and rate constants (lower panels) for H_2 and D_2 dissociation on Cu(001), as a function of temperature. The crossover from classical to quantum regimes is schematically indicated by the dash lines in (d).

The transmission coefficients $T_r(E)$, the total transmission probability $P_{tot}(T)$ at a given temperature T, the rate constants k, and the corresponding effective barrier E_b^* are deduced from the PES calculated at the DFT-GGA level. Further corrections can be made by introducing more accurate PES for the H_2–Cu(001) interactions (e.g., the PES calculated by the semi-empirical SRP-DFT approach[42–45]), the van der Waals corrections, or the interactions due to surface phonons. All these corrections may be taken as perturbations to the PES obtained by DFT-GGA calculations. As has been shown in Ref. [54] the perturbations or small changes to the original PES would only result in minor modifications on the transmission coefficients $T_r(E)$, and therefore the quantities derived based on $T_r(E)$. Consequently, the main results regarding the role of quantum tunneling in the dissociation kinetics of H_2 on Cu(001) qualitatively remain unchanged.

4. Conclusion

In summary, the activation and dissociation processes of H_2 molecules on the Cu(001) surface have been studied based on the first-principles calculations and the transfer matrix (TM) method. It is found that charge transfer from the substrate Cu atoms to H_2 plays an essential role in activating and breaking the H–H bond. Near the critical point of bond breaking, the adsorption configurations are characterized by the existence of two stationary states, and an abrupt change of H–H bond length is expected upon small perturbations to the translational motions of H_2. Using the MEP determined by the DFT calculations, the probabilities of H_2 molecules passing through the dissociation energy pathways are calculated using the TM method, which explicitly takes into account the effects of quantum tunneling. The probabilities and rate constants of dissociation due to the translational and the vibrational motions are evaluated and distinguished. Both translational and vibrational motions contribute nontrivially to the dissociation of H_2 at high temperatures. For the conditions when the Van't Hoff–Arrhenius relationship applies, the effective potential for the dissociation and adsorption of H_2 on Cu(001) is calculated. After the effects of quantum tunneling are considered, the barrier height is significantly reduced as compared with that of the barrier which treats the H_2 as a classical particle within the Born–Oppenheimer approximation. In the studies on the situation of thermal equilibrium and the non-equilibrium molecular beam of H_2, the calculated temperatures for the onset of measurable dissociation of H_2 on Cu(001) agree with the experiments. To further demonstrate the role of quantum tunneling, we have computed the effective barriers of dissociation for both H_2 and D_2, which are found to be comparable to the experimental data. The role of quantum effects is found to be remarkable in low-temperature region where the crossover

from the classical to quantum regimes is identified. The results are expected to be tested by future experiments.

Acknowledgements

Project supported by the National Natural Science Foundation of China (Grant Nos. 11474285 and 12074382). We are grateful to the staffs at the Hefei Branch of Supercomputing Center of Chinese Academy of Sciences, and the Hefei Advanced Computing Center for the support of supercomputing facilities.

References

[1] Swart I, de Groot F M F, Weckhuysen B M, Gruene P, Meijer G and Fielicke A 2008 *J. Phys. Chem. A* **112** 1139
[2] Lyu J Z, Andrey M L and Viktor N K 2019 *Chin. Phys. B* **28** 098801
[3] Wang Y L, Chen Y H and Wang Y H 2020 *Chin. Phys. B.* **29** 016801
[4] Salmeron M, Gale R J and Somorjai G A 1977 *J. Chem. Phys.* **67** 5324
[5] Kang H C and Weinberg W H 1995 *Chem. Rev.* **95** 667
[6] Anger G, Winkler A and Rendulic K D 1989 *Surf. Sci.* **220** 1
[7] Besocke K, Krahl-Urban B and Wagner H 1977 *Surf. Sci.* **68** 39
[8] Behm R J, Christmann K and Ertl G 1980 *Surf. Sci.* **99** 320
[9] Jardin J P, Desjonquères M C and Spanjaard D 1985 *Surf. Sci.* **162** 224
[10] Balooch M, Cardillo M J, Miller D R and Stickney R E 1974 *Surf. Sci.* **46** 358
[11] Tersoff J and Falicov L M 1981 *Phys. Rev. B* **24** 754
[12] Shen X, Li Y, Liu X, Zhang D, Gao J and Liang T 2017 *Phys. Chem. Chem. Phys.* **19** 3557
[13] Ferrin P, Kandoi S, Nilekar A U and Mavrikakis M 2012 *Surf. Sci.* **606** 679
[14] Alexander C S and Pritchard J 1972 *J. Chem. Soc., Faraday Trans. 1* **68** 202
[15] Rasmussen P B, Holmblad P M, Christoffersen H, Taylor P A and Chorkendorff I 1993 *Surf. Sci.* **287** 79
[16] Sun Q, Xie J J and Zhang T 1995 *Surf. Sci.* **338** 11
[17] Xie J J, Jiang P and Zhang K M 1994 *J. Phys.: Condens. Matter* **6** 7217
[18] Xie J J, Jiang P and Zhang K M 1996 *J. Chem. Phys.* **104** 9994
[19] Somers M F, McCormack D A, Kroes G J, Olsen R A, Baerends E J and Mowrey R C 2002 *J. Chem. Phys.* **117** 6673
[20] Christmann K, Ertl G and Pignet T 1976 *Surf. Sci.* **54** 365
[21] Hennig D, Wilke S, Löber R and Methfessel M 1993 *Surf. Sci.* **287** 89
[22] Payne S H, Kreuzer H J, Frie W, Hammer L and Heinz K 1999 *Surf. Sci.* **421** 279
[23] Smeets E W F, Voss J and Kroes G J 2019 *J. Phys. Chem. A* **123** 5395
[24] Harris J and Andersson S 1985 *Phys. Rev. Lett.* **55** 1583
[25] Harris J 1988 *Appl. Phys. A* **47** 63
[26] Halstead D and Holloway S 1988 *J. Chem. Phys.* **88** 7197
[27] Halstead D and Holloway S 1990 *J. Chem. Phys.* **93** 2859
[28] Nielsen U, Halstead D and Holloway S 1990 *J. Chem. Phys.* **93** 2879
[29] Darling G R and Holloway S 1994 *J. Chem. Phys.* **101** 3268
[30] Brenig W 1994 *Phys. Rev. Lett.* **73** 3121
[31] Kinnersley A D, Darling G R, Holloway S and Hammer B 1996 *Surf. Sci.* **364** 219
[32] Wang Z S, Darling G R and Holloway S 2000 *Surf. Sci.* **458** 63
[33] Dai J and Light J C 1997 *J. Chem. Phys.* **107** 1676
[34] Dai J and Light J C 1998 *J. Chem. Phys.* **108** 7816
[35] Miura Y, Kasai H and Diño W A 2002 *J. Phys.: Condens. Matter.* 14 L479
[36] Wiesenekker G, Kroes G J and Baerends E J 1996 *J. Chem. Phys.* **104** 7344
[37] Kroes G J, Baerends E J and Mowrey R C 1997 *Phys. Rev. Lett.* **78** 5383
[38] Kroes G J, Baerends E J and Mowrey R C 1997 *J. Chem. Phys.* **107** 3309
[39] McCormack D A, Kroes G J, Olsen R A, Baerends E J and Mowrey R C 1999 *J. Chem. Phys.* **110** 7008
[40] McCormack D A, Kroes G J, Olsen R A, Baerends E J and Mowrey R C 1999 *Phys. Rev. Lett.* **82** 1410
[41] Olsen R A, Busnengo H F, Salin A, Somers M F, Kroes G J and Baerends E J 2002 *J. Chem. Phys.* **116** 3841
[42] Díaz C, Pijper E, Olsen R A, Busnengo H F, Auerbach D J and Kroes G J 2009 *Science* **326** 832
[43] Sementa L, Wijzenbroek M, van Kolck B J, Somers M F, Al-Halabi A, Busnengo H F, Olsen R A, Kroes G J, Rutkowski M, Thewes C, Kleimeier N F and Zacharias H 2013 *J. Chem. Phys.* **138** 044708
[44] Marashdeh A, Casolo S, Sementa L, Zacharias H and Kroes G J 2013 *J. Phys. Chem. C* **117** 8851
[45] Kroes G J 2015 *J. Phys. Chem. Lett.* **6** 4106
[46] Sharada S M, Bligaard T, Luntz A C, Kroes G J and Nørskov J K 2017 *J. Phys. Chem. C* **121** 19807
[47] Kroes G J 2021 *Phys. Chem. Chem. Phys.* **23** 8962
[48] Jiang B and Guo H 2014 *J. Chem. Phys.* **141** 034109
[49] Zhu L J, Zhang Y L, Zhang L, Zhou X Y and Jiang B 2020 *Phys. Chem. Chem. Phys.* **22** 13958
[50] Lv S S, Liu X J and Shen X J 2022 *Surf. Sci.* **718** 122015
[51] Markland T E and Ceriotti M 2018 *Nat. Rev. Chem.* **2** 0109
[52] Ceriotti M, Fang W, Kusalik P G, McKenzie R H, Michaelides A, Morales M A and Markland T E 2016 *Chem. Rev.* **116** 7529
[53] Yang Y and Kawazoe Y 2019 *J. Phys. Chem. C* **123** 13804
[54] Bi C and Yang Y 2021 *J. Phys. Chem. C* **125** 464
[55] Schreiner P R 2020 *Trends Chem.* **2** 980
[56] Meisner J and Kästner J 2016 *Angew. Chem. Int. Ed.* **55** 5400
[57] Tierney H L, Baber A E, Kitchin J R and Sykes E C H 2009 *Phys. Rev. Lett.* **103** 246102
[58] Kyriakou G, Davidson E R M, Peng G, Roling L T, Singh S, Boucher M B, Marcinkowski M D, Mavrikakis M, Michaelides A and Sykes E C H 2014 *ACS Nano* **8** 4827
[59] Kresse G and Furthmüller J 1996 *Phys. Rev. B* **54** 11169
[60] Kresse G and Hafner J 1993 *Phys. Rev. B* **47** 558
[61] Perdew J P 1986 *Phys. Rev. B* **34** 7406
[62] Perdew J P, Burke K and Ernzerhof M 1996 *Phys. Rev. Lett.* **77** 3865
[63] Blöchl P E 1994 *Phys. Rev. B* **50** 17953
[64] Kresse G and Joubert D 1999 *Phys. Rev. B* **59** 1758
[65] Momma K and Izumi F 2011 *J. Appl. Crystallogr.* **44** 1272
[66] Monkhorst H J and Pack J D 1976 *Phys. Rev. B* **13** 5188
[67] Baroni S and Resta R 1986 *Phys. Rev. B* **33** 7017
[68] Schiff L I 1968 *Quantum Mechanics* (New York: McGraw-Hill) p. 268
[69] Bell R P 1980 *The Tunnel Effect in Chemistry* (London: Chapman and Hall)
[70] Chen B W J and Mavrikakis M 2020 *Catal. Sci. Technol.* **10** 671
[71] Yu M and Trinkle D R 2011 *J. Chem. Phys.* **134** 064111
[72] Ebrahimi M, Guo S Y, McNab I R and Polanyi J C 2010 *J. Phys. Chem. Lett.* **1** 2600
[73] Yang Y, Meng S and Wang E G 2006 *J. Phys.: Condens. Matter* **18** 10165
[74] Luo Y R 2005 *Experimental Data of Chemical Bond Energies* (Beijing: Science Press) p. 4
[75] Chapman S, Garrett B C and Miller W H 1975 *J. Chem. Phys.* **63** 2710
[76] Marcus R A and Coltrin M E 1977 *J. Chem. Phys.* **67** 2609
[77] Garrett B C and Truhlar D G 1983 *J. Chem. Phys.* **79** 4931
[78] Han E, Fang W, Stamatakis M, Richardson J O and Chen J 2022 *J. Phys. Chem. Lett.* **13** 3173
[79] Cheng Y H, Zhu Y C, Li X Z and Fang W 2023 *Chin. Phys. B* **32** 018201
[80] Büttiker M and Landauer R 1982 *Phys. Rev. Lett.* **49** 1739
[81] Wang Z C 2000 *Thermodynamics Statistical Physics*, 3rd Ed. (Beijing: Higher Education Press) pp. 271–273
[82] Lauhon L J and Ho W 2000 *Phys. Rev. Lett.* **85** 4566
[83] Sundell P G and Wahnström G 2004 *Phys. Rev. B* **70** 081403
[84] Zheng C Z, Yeung C K, Loy M M and Xiao X 2006 *Phys. Rev. Lett.* **97** 166101
[85] Cao G X, Nabighian E and Zhu X D 1997 *Phys. Rev. Lett.* **79** 3696